

Supporting information for

Spiranic BODIPYs: a ground-Breaking design to improve the energy transfer in molecular cassettes

Esther M. Sánchez-Carnerero,^a Leire Gartzia-Rivero,^b Florencio Moreno,^a
Beatriz L. Maroto,^a Antonia R. Agarrabeitia,^a María J. Ortiz,^a Jorge Bañuelos,^{*,b}
Iñigo López-Arbeloa,^b and Santiago de la Moya^{*,a}

^a*Departamento de Química Orgánica I, Facultad de Ciencias Químicas,
Universidad Complutense de Madrid, Ciudad Universitaria s/n, 28040, Madrid, Spain.
E-mail: santmoya@ucm.es*

^b*Departamento de Química Física, Universidad del País Vasco-EHU,
Apartado 644, 48080, Bilbao, Spain.
E-mail: jorge.banuelos@ehu.es*

Table of contents

| | |
|--|-----------|
| 1. General | S2 |
| 2. Synthetic procedures and characterization data | S4 |
| 3. Photophysical and computational results (Figs. S1-S4 and Table S1) | S5 |
| 4. ¹H NMR and ¹³C NMR spectra of 3 and 5 | S8 |

1. General

Synthesis

Common solvents were dried and distilled by standard procedures. All starting materials and reagents were obtained commercially and used without further purifications. Flash chromatography purifications were performed on silica gel 60 (60, 230-400 mesh ASTM). Thin-layer chromatography (TLC) was performed on silica gel plates (silica gel 60, F254, supported on aluminium). NMR spectra were recorded at 20 °C and the residual solvent peaks were used as internal standards. Complex spin-system signals were additionally simulated by using MestRe-C.¹ FTIR spectra were obtained from neat samples using the ATR technique. High resolution mass spectrometry (HRMS) was performed using the EI technique. Optical rotations were recorded in a Perkin-Elmer 241 polarimeter (*c* are expressed in g/100 mL). Elemental analyses were performed on a Leco CHNS-932 analyzer.

Photophysics

Standard abbreviations: Absorption maximum (λ_{ab}); fluorescence maximum (λ_{fl}); molar extinction coefficient at λ_{ab} (ϵ_{max}); fluorescence quantum yield (ϕ , FQY); mean fluorescence lifetime (τ); Stokes, or pseudo-Stokes when indicated, shift ($\Delta\nu_{St}$). Absorption and fluorescence spectra, as well as fluorescence-decay curves, were recorded in diluted solutions ($\sim 2 \cdot 10^{-6}$ M) of hexane (cut-off ~ 190 nm). UV-Vis absorption and fluorescence spectra were recorded on a Varian CARY 4E spectrophotometer and on a SPEX Fluorolog 3-22 spectrofluorimeter, respectively. ϕ values were obtained using starting PM567 ($\phi = 0.84$, in ethanol) as reference for Vis irradiation, and anthracene ($\phi = 0.27$, in ethanol) for UV. Values were calculated from corrected spectra (detector sensibility to the wavelength), and corrected by the refractive index of the solvent. Temperature-dependence measurements were performed using a liquid-hydrogen-cooled cryostat (Oxford), and an external electronic temperature-controller device for heating. Radiative-decay curves were registered with the time-correlated single-photon counting technique (Edinburgh Instruments FL920, with picosecond time-resolution). Fluorescence emission was

¹ MestRe-C: Cobas, C.; Cruces, J.; Sardina, J., MestRe-C; program version 2.3.

monitored at λ_{fl} upon direct excitation of the BODIPY at the Vis by means of a diode laser (PicoQuant LDH470) with 150 ps full width at half maximum (FWHM) pulses. τ values were obtained after the deconvolution of the instrumental response signal from the recorded decay curves by means of an iterative method. The goodness of the exponential fit was controlled by statistical parameters (chi-square, Durbin-Watson and analysis of the residuals).

Quantum mechanical calculations

Ground state geometries were optimized at the Density Functional Theory (DFT) using the hybrid B3LYP method, and the double valence basis set with diffuse and polarization functions (6-31+g*). The geometries were considered as energy minimum when the corresponding frequency analysis did not give any negative value. The absorption spectra were simulated by the Time-Dependent (TD) method. The solvent effect (hexane) was considered in the conducted theoretical simulations by means of the Polarizable Continuum Model (PCM). All the calculations were performed using the Gaussian 09² software as implemented in the computational cluster “arina” of the UPV/EHU.

² Gaussian 09: Frisch, M. J.; Trucks, G. W.; Schlegel, H. B.; Scuseria, G. E.; Robb, M. A.; Cheeseman, J. R.; Scalmani, G.; Barone, V.; Mennucci, B.; Petersson, G. A.; Nakatsuji, H.; Caricato, M.; Li, X.; Hratchian, H. P.; Izmaylov, A. F.; Bloino, J.; Zheng, G.; Sonnenberg, J. L.; Hada, M.; Ehara, M.; Toyota, K.; Fukuda, R.; Hasegawa, J.; Ishida, M.; Nakajima, T.; Honda, Y.; Kitao, O.; Nakai, H.; Vreven, T.; Montgomery, J. A., Jr.; Peralta, J. E.; Ogliaro, F.; Bearpark, M.; Heyd, J. J.; Brothers, E.; Kudin, K. N.; Staroverov, V. N.; Kobayashi, R.; Normand, J.; Raghavachari, K.; Rendell, A.; Burant, J. C.; Iyengar, S. S.; Tomasi, J.; Cossi, M.; Rega, N.; Millam, N. J.; Klene, M.; Knox, J. E.; Cross, J. B.; Bakken, V.; Adamo, C.; Jaramillo, J.; Gomperts, R.; Stratmann, R. E.; Yazyev, O.; Austin, A. J.; Cammi, R.; Pomelli, C.; Ochterski, J. W.; Martin, R. L.; Morokuma, K.; Zakrzewski, V. G.; Voth, G. A.; Salvador, P.; Dannenberg, J. J.; Dapprich, S.; Daniels, A. D.; Farkas, Ö.; Foresman, J. B.; Ortiz, J. V.; Cioslowski, J.; Fox, D. J. Gaussian, Inc., Wallingford CT, 2009.

2. Synthetic procedure and characterization data

A mixture of commercial PM567 (2,6-diethyl-1,3,5,7,8-pentamethylBODIPY, 60.0 mg, 0.188 mmol) and aluminum chloride (62.1 mg, 0.465 mmol) in dry CH₂Cl₂ (6 mL) was refluxed under argon atmosphere until reaction completion (reaction monitoring by TLC). The mixture was cooled down to room temperature and, then, a solution of 2-naphthol (97.6 mg, 0.677 mmol; for obtaining **3**), or (*R*)-VAPOL (182.2 mg, 0.338 mmol; for obtaining **5**), in anhydrous acetonitrile (3 mL) was added dropwise. The resulting mixture was stirred at r.t. for additional 6 h, washed with brine (1×6 mL) and dried over anhydrous Na₂SO₄. After filtration and solvent evaporation under reduced pressure, the obtained residue was purified by flash chromatography (hexane/Et₂O 8:2 for **3** and hexane/acetone 95:5 for **5**) to afford the corresponding *O*-BODIPY.

O-BODIPY 3: Yield: 81 mg, 76 %. $R_f = 0.27$ (hexane:Et₂O 8:2). ¹H NMR (CDCl₃, 300 MHz) δ 7.67 (d, $J = 8.0$ Hz, 2H), 7.59 (d, $J = 8.9$ Hz, 2H), 7.42 (d, $J = 8.1$ Hz, 2H), 7.31 (t app, $J = 7.5$ Hz, 2H), 7.22 (t app, $J = 7.4$ Hz, 2H), 7.03 (dd, $J = 8.9, 2.3$ Hz, 2H), 6.65 (d, $J = 2.0$ Hz, 2H), 2.74 (s, 3H), 2.59 (s, 6H), 2.40 (s, 6H), 2.29 (q, $J = 7.5$ Hz, 4H), 0.93 (t, $J = 7.5$ Hz, 6H) ppm. ¹³C NMR (CDCl₃, 75 MHz) δ 154.6, 152.7, 139.4, 136.4, 134.8, 133.1, 132.3, 128.5, 128.3, 127.2, 126.6, 125.2, 122.6, 121.9, 112.5, 17.1, 16.9, 14.8, 14.5, 12.7 ppm. FTIR ν 1551, 1316 cm⁻¹. HRMS m/z 566.3098 (calcd. for C₃₈H₃₉BN₂O₂ 566.3105). Elemental analysis % 80.53 C, 6.91 H, 4.92 N. (calcd. for C₃₈H₃₉BN₂O₂ 80.56 C, 6.94 H, 4.94 N).

O-BODIPY 5: Yield: 85 mg, 55%. $R_f = 0.35$ (hexane:acetone 9:1). $[\alpha]_D^{20} -2601$ (c 0.079 CHCl₃). ¹H NMR (CDCl₃, 300 MHz) δ 9.87 (d, $J = 8.4$ Hz, 2H), 7.80 (d, $J = 7.8$ Hz, 2H), 7.65 (d, $J = 8.7$ Hz, 2H), 7.60 (d, $J = 8.8$ Hz, 2H), 7.48 (dd, $J = 7.8, 6.9$ Hz, 2H), 7.37 (dd, $J = 7.8, 7.7, 1.4$ Hz, 2H), 7.31 (s, 2H), 7.06 (t, $J = 7.3$ Hz, 2H), 6.92 (dd, $J = 7.7, 7.4$ Hz, 4H), 6.64 (d, $J = 7.2$ Hz, 4H), 2.57 (s, 3H), 2.11 (s, 6H), 1.98 (m, 4H), 1.65 (s, 6H), 0.49 (t, $J = 7.5$ Hz, 6H) ppm. ¹³C NMR (CDCl₃, 75 MHz) δ 155.4, 153.2, 142.0, 141.3, 138.8, 135.8, 133.8, 133.5, 132.7, 132.4, 130.7, 129.8, 128.9, 127.7, 127.5, 127.3, 127.2, 126.9, 125.9, 125.6, 125.3, 123.8, 122.9, 17.6, 16.9, 14.3, 14.2, 13.1 ppm. FTIR ν 1556, 1381 cm⁻¹. HRMS m/z 816.3879 (calcd. for C₅₈H₄₉BN₂O₂ 816.3887). Elemental analysis % 85.25 C, 6.01 H, 3.40 N (calcd. for C₅₈H₄₉BN₂O₂ 85.28 C, 6.05 H, 3.43 N).

3. Photophysical and computational results (Figs. S1-S4 and Table S1)

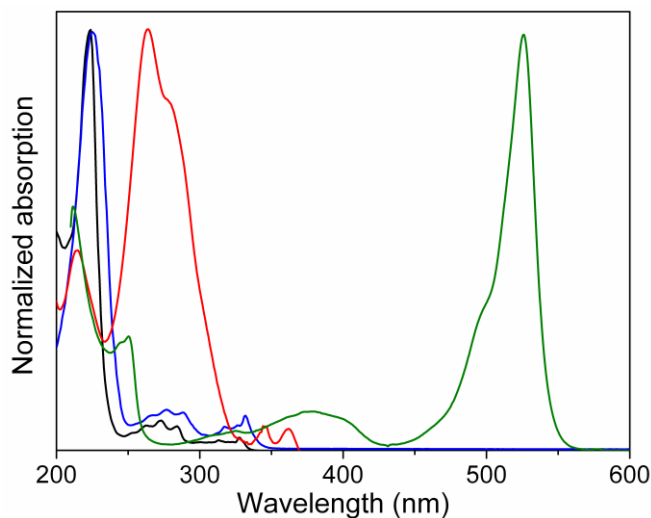


Figure S1. Absorption spectra of 2-naphthol (black), BINOL (blue), VAPOL (red) and PM567 (green) in hexane.

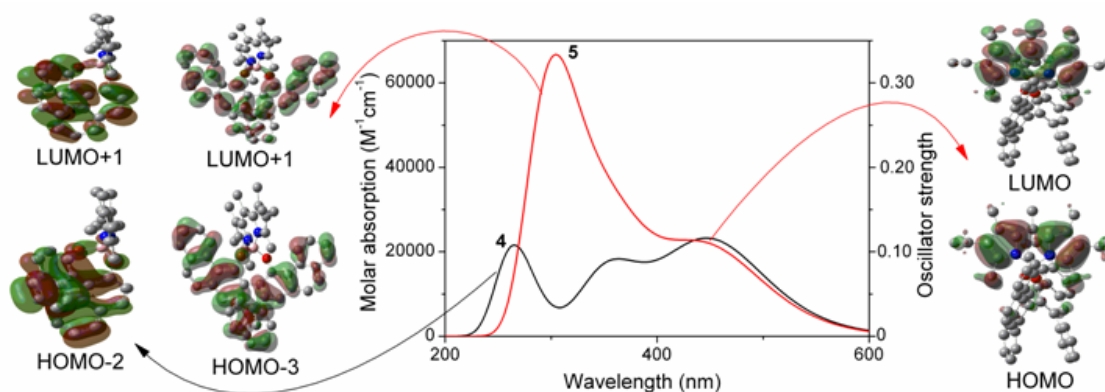


Figure S2. Theoretically simulated absorption (TD B3LYP/6-31+g*) of **4** and **5**, and main molecular orbitals involved in the absorption bands (TD calculations overestimate the energy gap, and underestimate the probability of the less-energetic transitions).

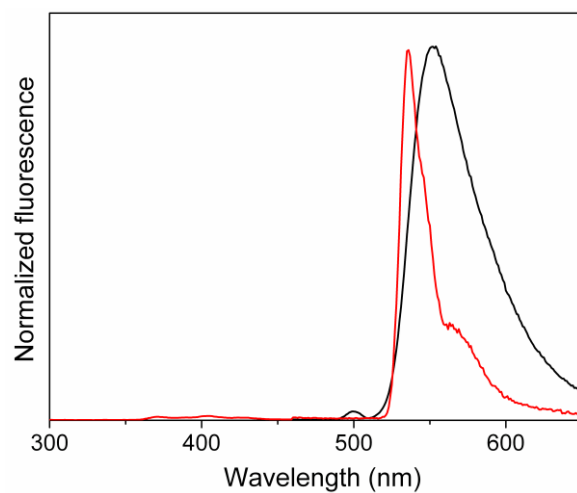


Figure S3. Normalized fluorescence spectra of **4** upon UV irradiation (BINOL excitation) at 293 K (black) and 77 K (red, blue shift and narrow shape due to cooling effect).

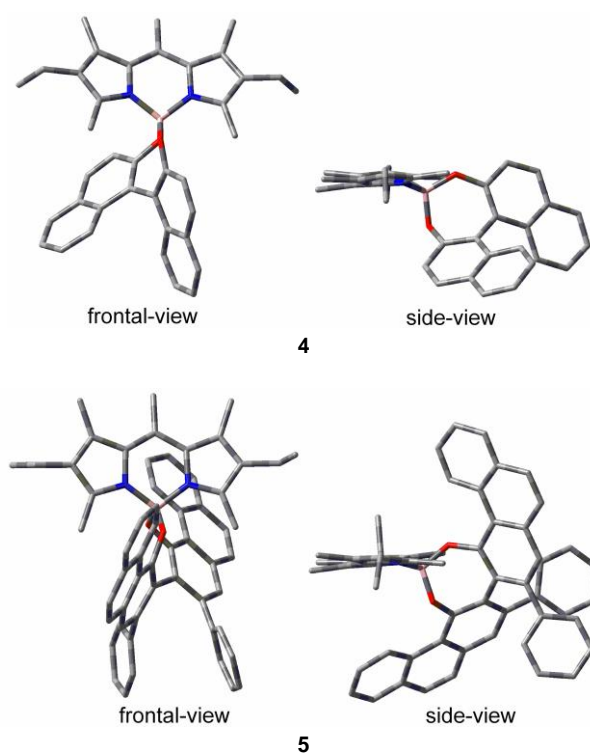


Figure S4. B3LYP/6-31+g* ground-state geometries of **4** and **5**.

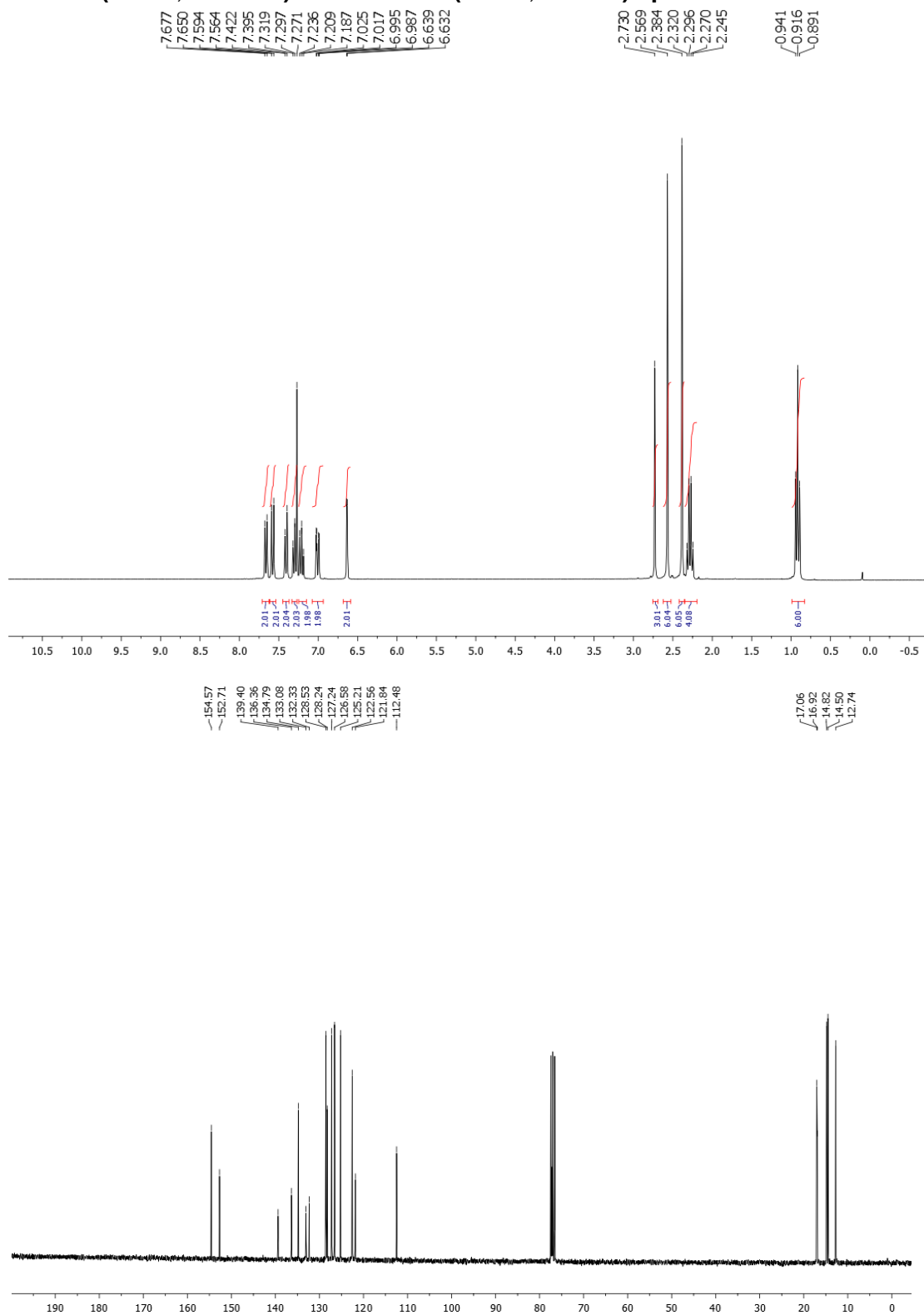
Table S1. Cassette behavior of **3-5** in hexane.

| Compound | λ_{ab} (nm) | $\epsilon_{\max} \cdot 10^{-4}$ (M ⁻¹ cm ⁻¹) | λ_{fl} (nm) | ϕ | τ^a (ns) | ν_{St} (cm ⁻¹) |
|----------------------|------------------------|--|------------------------|---------------------|-------------------|-----------------------------------|
| 3 | 523.0 | 3.8 | 540.0 ^a | 0.56 ^a | 5.44 ^c | 600 ^a |
| | 250.0 | 9.4 | 398.0 ^b | 0.19 ^b | | 14880 ^b |
| 4 | 523.0 | 6.7 | 546.0 ^{a,b} | 0.89 ^{a,b} | 5.99 | 800 ^a |
| | 225.0 | 8.0 | | | | 26130 ^{b,d} |
| 5^e | 530.0 | 6.8 | 552.0 ^{a,b} | 0.94 ^{a,b} | 6.54 | 750 ^a |
| | 288.0 | 9.3 | 404.0 ^b | 0.006 ^b | | 9970 ^b |
| | | | | | | 16600 ^{b,d} |

^aUpon Vis irradiation (470 nm). ^bUpon UV irradiation (250 nm). ^cAveraged mean lifetime from the biexponential fit (0.73 ns, 11%; 6.03 ns, 89%). ^dPseudo-Stokes shift. ^eSimilar results are obtained when chloroform is used as the solvent instead of hexane.

4. ^1H NMR and ^{13}C NMR spectra of 3 and 5

^1H NMR (CDCl_3 , 300 MHz) and ^{13}C NMR (CDCl_3 , 75 MHz) spectra of 3



¹H NMR (CDCl₃, 300 MHz) and ¹³C NMR (CDCl₃, 75 MHz) spectra of 5

